Hindawi Publishing Corporation
Advances in Materials Science and Engineering
Volume 2016, Article ID 1750105, 10 pages
http://dx.doi.org/10.1155/2016/1750105

Research Article

Electropolished Titanium Implants with a Mirror-Like Surface Support Osseointegration and Bone Remodelling

Cecilia Larsson Wexell,[1,2,3] Furqan A. Shah,[2,3] Lars Ericson,[4] Aleksandar Matic,[5] Anders Palmquist,[2,3] and Peter Thomsen[2,3]

[1]*Department of Oral and Maxillofacial Surgery, Public Dental Service, Region Västra Götaland, SÄS, Borås, Sweden*
[2]*Department of Biomaterials, Institute of Clinical Sciences, Sahlgrenska Academy at University of Gothenburg, Göteborg, Sweden*
[3]*BIOMATCELL VINN Excellence Center of Biomaterials and Cell Therapy, Göteborg, Sweden*
[4]*Department of Medical Biochemistry and Cell Biology, Sahlgrenska Academy at University of Gothenburg, Göteborg, Sweden*
[5]*Department of Physics, Chalmers University of Technology, Göteborg, Sweden*

Correspondence should be addressed to Cecilia Larsson Wexell; cecilia.larsson@vgregion.se

Received 24 August 2016; Revised 29 September 2016; Accepted 16 November 2016

Academic Editor: Michele Iafisco

This work characterises the ultrastructural composition of the interfacial tissue adjacent to electropolished, commercially pure titanium implants with and without subsequent anodisation, and it investigates whether a smooth electropolished surface can support bone formation in a manner similar to surfaces with a considerably thicker surface oxide layer. Screw-shaped implants were electropolished to remove all topographical remnants of the machining process, resulting in a thin spontaneously formed surface oxide layer and a smooth surface. Half of the implants were subsequently anodically oxidised to develop a thickened surface oxide layer and increased surface roughness. Despite substantial differences in the surface physicochemical properties, the microarchitecture and the composition of the newly formed bone were similar for both implant surfaces after 12 weeks of healing in rabbit tibia. A close spatial relationship was observed between osteocyte canaliculi and both implant surfaces. On the ultrastructural level, the merely electropolished surface showed the various stages of bone formation, for example, matrix deposition and mineralisation, entrapment of osteoblasts within the mineralised matrix, and their morphological transformation into osteocytes. The results demonstrate that titanium implants with a mirror-like surface and a thin, spontaneously formed oxide layer are able to support bone formation and remodelling.

1. Introduction

On titanium, the surface oxide layer (TiO_2) has been suggested to control the biological response and in vivo performance when used as bone anchored implant [1]. Various combinations of mechanical, thermal, chemical, and electrochemical surface treatments have been used to systematically study and determine the surface characteristics of physiological relevance in an effort to reduce the initial healing time and allow predictable long-term clinical performance [2, 3]. Important advances in developing novel surface properties on biomaterials such as dental implants have been made and experimental studies demonstrate differences in tissue response to different surface modifications. Electropolishing is an electrochemical technique often used to obtain an improved surface finish by controlled dissolution of the surface layer of the metal. A lower bone-implant contact has been reported for smooth electropolished surfaces with a thin surface oxide at early healing periods, that is, 1–7 weeks in rabbit cortical bone, compared to anodised surfaces having relatively thicker surface oxide [4, 5].

Having complex hierarchical architecture [6, 7], the mechanical properties of bone depend on bone density, microstructure, and ultrastructure [8]. The bone mineral density distribution reflects bone turnover, mineralisation kinetics, and the average tissue age, with an apparent heterogeneity of mineralisation in different bone packets originating from two simultaneous processes: (i) continuous

resorption and formation by bone multicellular units and (ii) mineralisation of the newly deposited bone packets via a kinetic process [9]. In mineralising zebrafish fin rays, submicron-sized packages of amorphous calcium phosphate spheres formed inside the cells are delivered to the extracellular collagenous matrix followed by their transformation into crystalline platelets of carbonated hydroxyapatite [10]. Similar mineral packets, described as *calcospherulites*, are also observed in close association with osteoblastic-osteocyte lacunae on bone surfaces [11]. The organic component of the matrix strongly influences the fracture mechanics of bone [12], where both the collagen content and collagen cross-linking play a critical role [13]. On the other hand, the optimal amount of mineral maximising both toughness and strength of a single mineralised collagen fibril, while maintaining a relatively low density, is only ~30% [14].

The interfacial tissue adjacent to titanium implant surfaces has a heterogeneous appearance with a combination of mineralised bone, not mineralised bone, and soft tissue regions, similar to ordinary bone tissue [15]. The amount of mineralised bone in direct contact with conventional machined surfaces is about 56–85% after 1–16 years of clinical function [16]. While intentionally roughened surfaces, for example, with a thickened surface oxide layer, produced by anodic oxidation result in a reinforcement of the bone response [2], whether smooth titanium surfaces allow bone formation/remodelling to progress in the same manner as highly textured surfaces is rarely investigated. Here, it was hypothesised that, given adequate primary stability (e.g., with a threaded implant design and a standard surgical protocol), a smooth, relatively featureless, mirror-like titanium surface could support osseointegration and bone remodelling.

2. Materials and Methods

2.1. Implant and Surface Preparation. Threaded screw-shaped implants (3.75 mm diameter, 4.0 mm length) were machined from a commercially pure (99.7%) titanium rod, grade 1. Two types of surfaces were prepared: (i) electropolished (Ep), and (ii) electropolished + anodised (Ep+An) types. In the first step, all implants were electrochemically polished to remove the amorphous and plastically deformed surface layer and irregularities resulting from the machining process. In an electrolytic bath consisting of 600 mL methanol, 350 mL, *n*-butanol, and 60 mL perchloric acid, held at −30°C, a voltage of 22.5 V was applied for 5 min. Electrolytic residues were removed by rinsing in methanol. Half of the implants further underwent anodic oxidation (anodisation) in 1 M acetic acid at room temperature and a voltage of 80 V. Galvanostatic (current) control at 60 mA/cm^2 was applied until the preset potential was reached, after which the process was controlled potentiostatically. The anodisation was terminated after 5–10 min when the current had decreased to 2% of the initial value. The anodised samples were rinsed in deionised water and ethanol. All implants were cleaned ultrasonically in *n*-butanol for 10 min and ethanol for 3 × 10 min and autoclaved.

2.2. Surface Characterisation. The surface morphology was examined by scanning electron microscopy (SEM; Versa 3D dual beam FIB/SEM, FEI Company, Netherlands) operated at 10 kV. The thickness of the surface oxide layer on the Ep+An surface was further evaluated by the *slice-and-view* function. An area of interest was protected with a thin (1 μm) layer of platinum. A large cross section was milled using high Ga^+ ion beam current and subsequent polishing by decreasing ion beam current followed by SEM imaging [17, 18].

Surface topography was analysed using white light interference microscopy (Rough Surface Tester Light Interferometer, WYKO Corporation, Tucson, AZ) operating in the vertical scanning mode. The raw data were processed by tilt and cylindrical shape correction prior to analysis. The surface composition was analysed by scanning Auger electron spectroscopy (AES, Perkin Elmer PHI 600, USA). AES survey spectra (30–1630 eV) were recorded at two spots (100 μm diameter) located in the threaded part on two samples from each group. Relative concentrations (atomic % in the analysed volume) of the detected elements were estimated from peak heights in the different spectra, after corrections based on elemental sensitivity factors. In order to estimate the surface oxide thicknesses, depth profiles were measured by combining AES analysis and Ar^+ ion sputter etching at two spots (10 μm diameter) on one sample from each group.

2.3. Animal Surgery and Sample Preparation. Seven adult New Zealand white rabbits, weighing 3-4 kg, were used. The experiment was approved by the local Animal Ethics Committee at the University of Gothenburg. The animals were anaesthetised by a combination of fluanisone and fentanyl (Hypnorm® Injection, VetaPharma Ltd., Leeds, UK; 1 mL/kg body weight) administered intramuscularly and diazepam (Actavis Group hf, Hafnarfjordur, Iceland; 2.5 mg/kg body weight) administered intraperitoneally and lidocaine (5% Xylocain®, AstraZeneca AB, Sweden) as local anaesthetic in the skin and the periosteum. Low-speed drilling with round-bur, twist drills, prethreading, and continuous irrigation with saline (all according to a standard clinical surgical protocol) was used and each animal received both implant types, one in each proximal tibial metaphysis. All implants were stable after insertion. The animals were allowed to move freely and were fed *ad libitum*. At 12 weeks, the animals were euthanised by an overdose of sodium pentobarbital intravenously followed by perfusion of 2.5% glutaraldehyde in 0.05 M sodium cacodylate buffer, pH 7.2, via the left heart ventricle. The implants together with the surrounding bone were removed *en bloc* and further immersed in glutaraldehyde for 24 hours and then postfixed in 1% osmium tetroxide for another two hours. After dehydration, in a graded series of ethanol, the specimens were embedded in plastic resin (LR White, London Resin Company, UK). The blocks were bisected longitudinally by sawing [19].

2.4. Bone Microstructure and Direct Visualisation of Osteocyte Morphology. One half-block was polished using 400–2400 grit SiC paper and examined in a Quanta 200 environmental SEM (FEI Company, Netherlands) operated in the

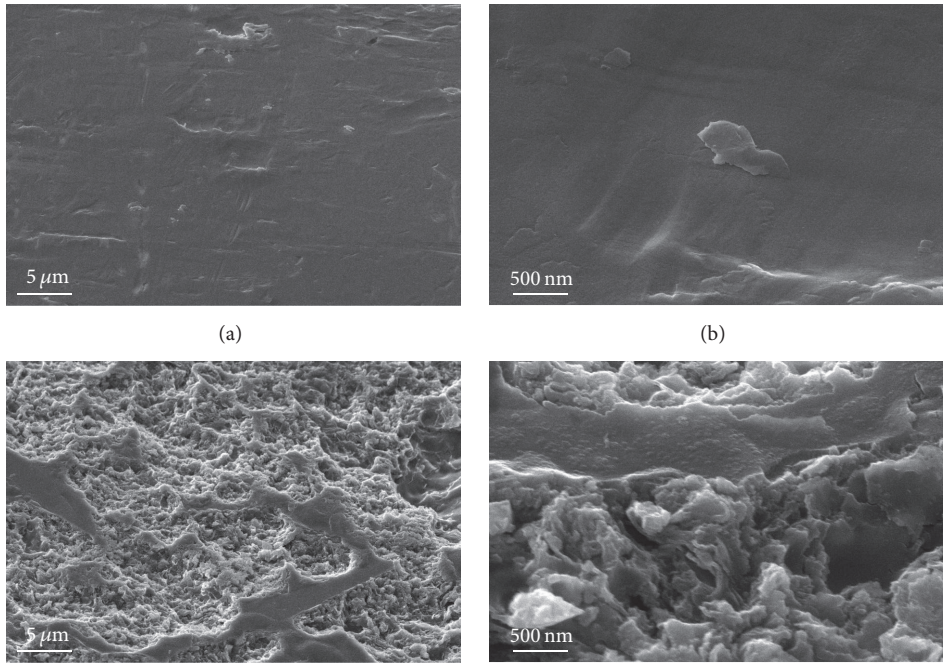

Figure 1: Surface topography of the (a-b) Ep and (c-d) Ep+An implant surfaces.

backscattered electron (BSE) mode at 20 kV and 0.5 Torr water vapour pressure. The osteocyte lacunocanalicular network (Ot-LCN) was exposed by resin cast etching for high-resolution visualisation [20]. Briefly, the resin-embedded blocks were polished using 400–4000 grit SiC polishing paper, followed by sequential immersion in 9% orthophosphoric acid and 5% sodium hypochlorite. After overnight drying, the samples were sputter-coated with a 10 nm thick layer of Au and examined by secondary SEM (Ultra 55 FEG SEM, Leo Electron Microscopy Ltd., UK), at 5 kV accelerating voltage and 5 mm working distance.

2.5. Interfacial Tissue Composition. The other half-block was used for Raman spectroscopy in order to investigate the composition of the interfacial tissue (5–10 μm from the implant surface) adjacent to both implant surfaces. The native bone in the same tissue-implant block was analysed as reference. Spectra were collected at room temperature by a nitrogen cooled charge-coupled device (CCD) detector connected to a Dilor XY spectrometer (Horiba, Jobin Yvon GmbH), equipped with a 676 nm Ar/Kr laser operated at ~100 mW, with a 100x objective, 600 groove/mm grating, 300 mm focal length, and pinhole size of 500 μm. Three different positions were analysed for each group, and 10 acquisitions were made at each position with an integration time of 20 s each. Raw spectra were processed using the Background Correction program [21] for MATLAB R2013b (MathWorks Inc., Natick, MA). The wavenumber axis was adjusted so that $\nu_1 PO_4^{3-}$ peaks in all spectra corresponded to ~959 cm^{-1}. Noise removal was performed using a Fast Fourier Transform (FFT) algorithm and the baseline-corrected spectra were normalised to $\nu_1 PO_4^{3-}$ band intensity in Plot (http://plot.micw.eu/).

2.6. Interfacial Tissue Ultrastructure. For the electropolished (Ep) implants only, the resin-embedded implant was mechanically separated from the surrounding tissue, and the tissue was reembedded using the same resin. Using glass knives, 1 μm thick sections were made in order to identify appropriate locations for subsequent preparation of ultrathin sections (<100 nm) using diamond knives and contrast stained with uranyl acetate and lead citrate for transmission electron microscopy (TEM; Philips EM 400 and Zeiss CEM 902). Owing to the extremely roughened nature of the Ep+An surface, it was not possible to cleanly separate the bone tissue from the implant for subsequent sectioning for TEM.

3. Results

3.1. Surface Characterisation. The electropolished (Ep) surface was smooth on the micro- and nanoscale, showing only rare and subtle traces from the machining process. The electropolished + anodised (Ep+An) surface, in comparison, was considerably roughened, displaying submicron porosity with interspersed, smoother, protruding areas (Figure 1). Interference microscopy confirmed the visual differences in surface roughness, with S_a values of 71 ± 6 nm (Ep) and 444 ± 167 nm (Ep+An).

By AES depth profiling, the mean thickness of the surface oxide was found to be 4-5 nm at the Ep surface, and 180 nm at the Ep+An surface. In cross section, the surface oxide

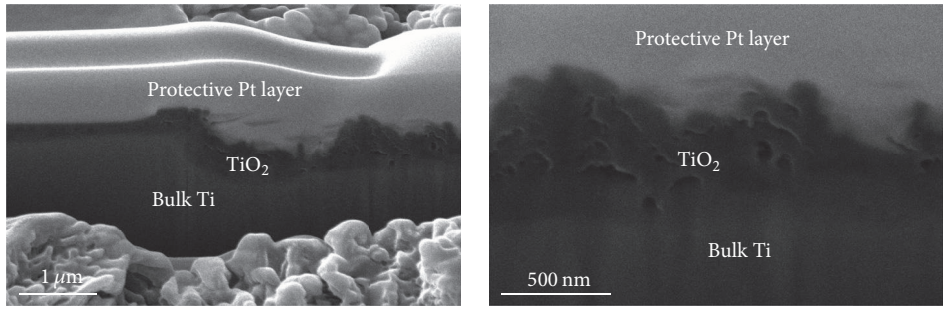

(a) (b)

Figure 2: Focused ion beam (FIB) cross-sectional view of the Ep+An implant surface.

layer was porous in structure, with a majority of pores at the interface between the bulk metal and the surface oxide (Figure 2). The cross-sectional thickness of the surface oxide layer varied between 100 and 500 nm, where the thinner nonporous regions were confined exclusively to the smoother surface regions. The surface oxide layer of the Ep surface could not be imaged in cross section by FIB-SEM. The composition of both surfaces, also evaluated by AES, was mainly titanium, oxygen, and carbon, with similar trace amounts of Ca, P, Na, Cl, Si, and S.

3.2. Bone Microstructure and Visualisation of Osteocyte Morphology. High amounts of mature, mineralised, lamellar bone were observed around both implant types after 12 weeks. Within the implant threads, the newly formed bone exhibited an osteonal structure, indicative of bone remodelling following an initial formation of woven bone. The BSE Z-(atomic number) contrast can be interpreted as an indicator of bone tissue mineralisation. Bone inside the implant threads exhibited a slightly lower Z-contrast than the native bone outside the threads, though no qualitative differences were noticed between the two implant surfaces (Figures 3(a)-3(b)).

Following resin cast etching, the vast Ot-LCN was observed in close proximity to the implant surface (Figures 3(c)–3(f)). In the native bone, the osteocytes were generally aligned parallel to the longitudinal axis of the tibia and the lamellar direction. In contrast, the osteocytes within the implants threads exhibited a comparatively rounded morphology with seemingly higher numbers of canaliculi per osteocyte lacuna compared to osteocytes in the native bone and were aligned along successive lamellae that followed the implant surface contour. Again, differences were not observed between the two surfaces. It must however be noted that, by resin cast etching, osteocytes and canaliculi are not directly visualised, but what is observed is the resin that had infiltrated and filled these spaces.

3.3. Interfacial Tissue Composition. Typical Raman signatures for bone (Figure 4(a)) were observed at the interfacial tissue (Figures 4(c) and 4(e)) adjacent to both implant types. The composition of the interfacial tissue adjacent to both implant types was comparable and approximately similar to mature, mineralised, native bone. The inverse full width at half maximum (1/FWHM) values of $\nu_1 PO_4^{3-}$ band suggested slightly lower mineral crystallinity at the interfacial tissue (versus the native bone) for both implant surfaces (Figure 4(d)). Phenylalanine (Phe) and Tyrosine (Tyr) signals at the Ep surface were slightly higher than at the Ep+An surface, suggesting subtle variations in the organic phase of the bone adjacent to the two surfaces.

3.4. Interfacial Tissue Ultrastructure. Using transmission electron microscopy, the various stages of bone formation, from osteoid deposition by osteoblasts (Ob) to the morphological transformation of osteoblasts into osteocytes (Ot) simultaneous with the initiation and progression of mineralisation, could be observed adjacent to the Ep implant surface (Figure 5). Collagen fibrils showed a characteristic 67 nm crossbanding pattern and were aligned parallel to the implant surface. Osteocytes appeared to make direct contact with the implant surface through numerous dendritic extensions within canaliculi. Supporting the observations made by resin cast etching, TEM confirmed the presence of osteocyte processes reaching and directly contacting the implant surface.

4. Discussion

The initial stability, survival, and eventual success of an implant are dependent on a variety of factors including the surgical technique, the quality of the adjacent bone, and the macrogeometry and surface physicochemical properties of the implant [22]. Bone quality is determined by a combination of the unique hierarchical structure and the composition [23]. Following a surgical trauma, for example, insertion of an implant, a healing process is initiated where bone formation progresses from a poorly organised woven bone phase to a remodelled lamellar structure [24], where the tissue is highly organised on the micrometre and nanometre length scales in adaptation to local biomechanical conditions [15, 25, 26].

This work explored the hypothesis that commercially pure titanium implants with a smooth, mirror-like surface obtained by electropolishing (but without any further processing) could support bone apposition and remodelling in a manner similar to electropolished and subsequently anodised

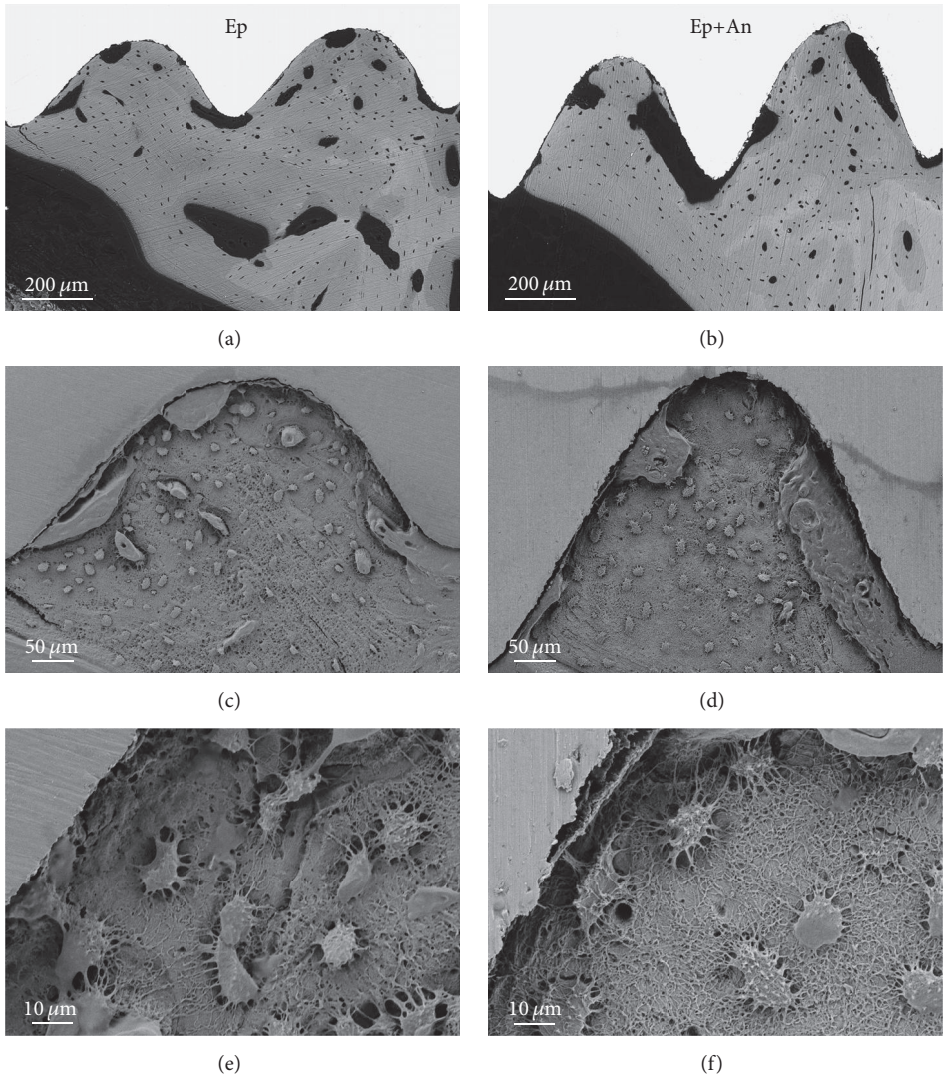

Figure 3: Backscattered electron scanning electron microscopy. High amounts of well-mineralised bone are observed within and outside the (a) Ep and (b) Ep+An implant threads. (c–f) Resin cast etching and direct visualisation of osteocytes forming a vast network of the lacunocanalicular system in close proximity to the (c, e) Ep and (d, f) Ep+An implant surfaces.

implants having a 45-fold higher oxide thickness and 6-fold higher surface roughness, provided that primary stability can be ensured. Previous morphological studies have demonstrated a lower degree of bone-implant contact for merely electropolished (Ep) implants compared to electropolished + anodised (Ep+An) implants in the same animal model at 1–7 weeks of healing [4, 5]. Therefore, 12 weeks of healing was chosen as a midterm healing period, by which signs of remodelling and reorganisation of the early-formed woven bone into organised lamellar bone may become apparent.

Other recent studies have demonstrated the role of a thickened surface oxide layer, exhibiting a combined microtopography and nanotexture, in achieving stronger biomechanical anchorage of screw-shaped titanium implants [27]. However, despite considerable differences in surface oxide thickness and surface roughness between the Ep and Ep+An implant surfaces, both exhibited similar patterns of bone formation and remodelling. On the ultrastructural level, organic matrix deposition by osteoblasts, initiation and progression of mineralisation, the entrapment of osteoblasts within the mineralised matrix, and their subsequent morphological transformation into osteocytes were visualised directly. To a large extent, these structural changes were comparable for the two surfaces. The microstructure and composition of newly formed bone were evaluated by BSE-SEM and Raman spectroscopy. While the mineral distribution within the newly formed bone showed a comparable heterogeneous distribution of grey level intensities on BSE-SEM images, no major alterations were detected in the composition of the interfacial tissue, for example, mineral crystallinity, the apatite-to-collagen ratio, and the degree of carbonation.

The electropolishing procedure was able to remove the machining grooves/undulations, making the surface almost

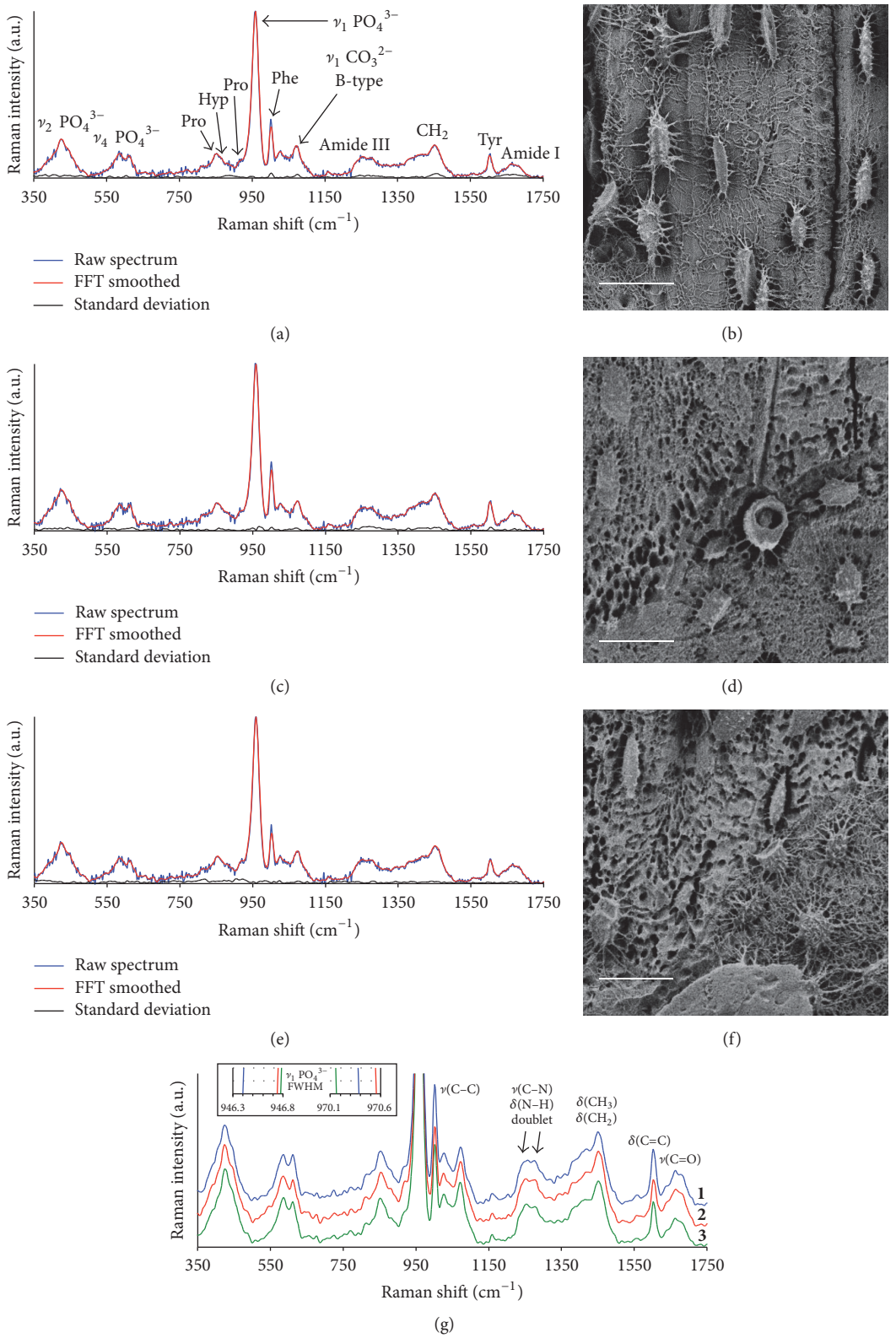

FIGURE 4: Raman spectra of the (a) native bone and the interfacial tissue 5–10 μm from the (c) Ep and (e) Ep+An implant surfaces. (b) Osteocytes in the native bone are aligned parallel to the lamellar direction. The interface between the bone tissue contained within the (d) Ep and (f) Ep+An implant threads and the native bone outside the implant threads. Scale bars = 20 μm. (g) Raman spectra (y-axis shifted) for the three groups: bone, anodised, and electropolished. Inset in (g): Raman spectra (overlaid/not y-axis shifted, x-axis truncated) showing the half-maximum region of $\nu_1 PO_4^{3-}$ at 960 cm^{-1}. The difference in full width at half maximum suggests minor differences in mineral crystallinity.

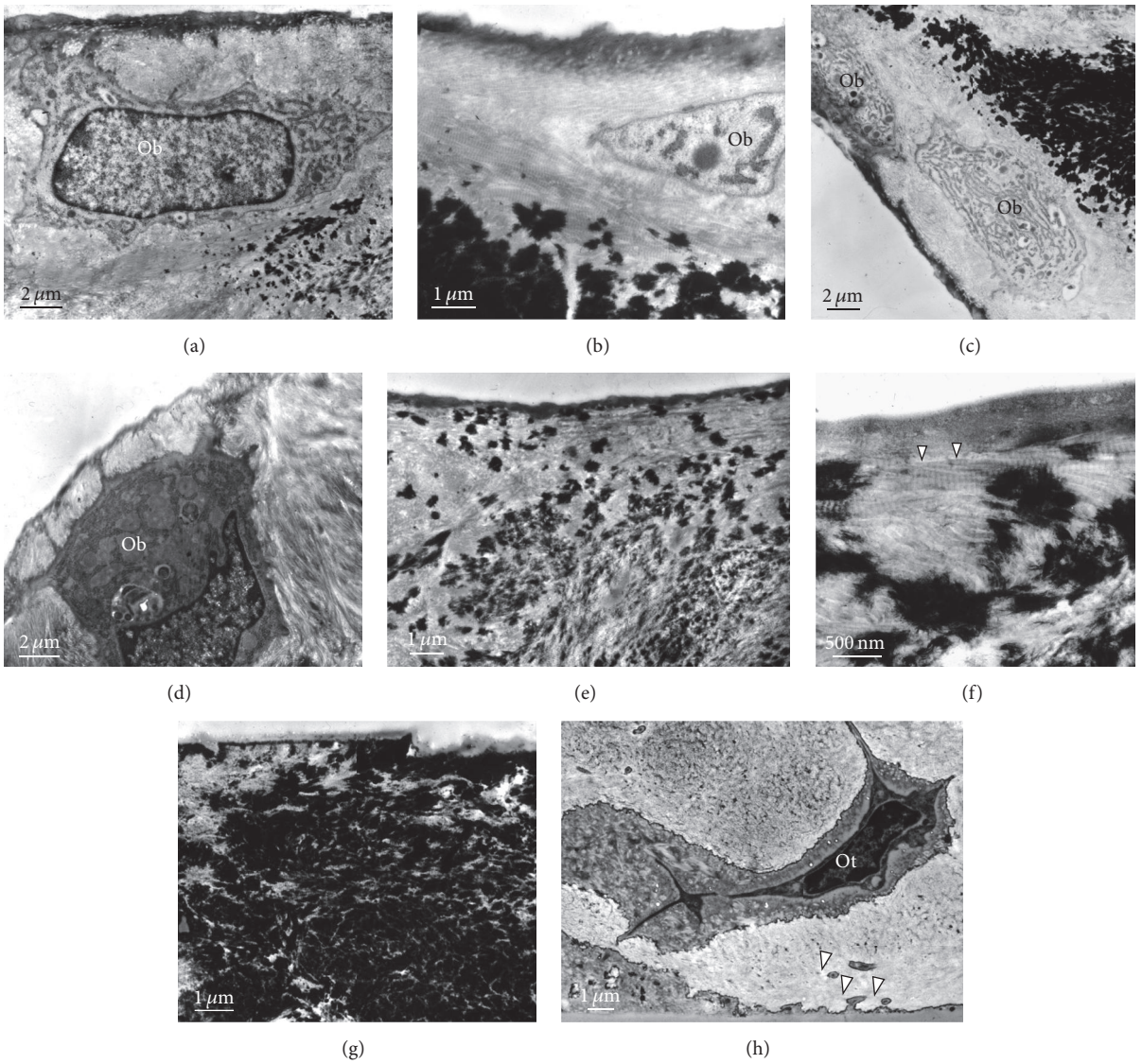

Figure 5: Transmission electron microscopy. The various stages of bone formation adjacent to the Ep surface could be observed at 12 weeks of healing. (a–c) At the bone-implant interface, osteoblasts (Ob) produce an unmineralised extracellular matrix, the osteoid, which undergoes progressive mineralisation. (d) Collagen fibrils are aligned parallel to the osteoblast surface. (e) Early mineralisation stage with patchy distribution of bone apatite (dark areas). (f) In high-resolution, the characteristic 67 nm cross-striated pattern of collagen fibrils (white arrows) can be observed, with accumulation of intra- and interfibrillar mineral. (g) Late mineralisation stage with diffuse distribution of bone apatite (dark areas). (h) An osteocyte (Ot) embedded within the mineralised matrix lies in close proximity to the implant surface with several dendritic processes residing within canaliculi (white arrows), sectioned longitudinally as well as transversally, extending towards the implant surface.

completely smooth on the submicron and nanometre levels with a surface oxide layer thickness of 4-5 nm, in agreement with earlier studies [4, 5]. The subsequent anodisation increased the thickness of the surface oxide layer by a factor of 100–250 and resulted in a fine micrometre to submicron scale topography (S_a = ~450 nm) and a heterogeneous surface, displaying porous and interspersed smoother areas. Chemical analysis demonstrated that the composition of both surfaces, also evaluated by AES, was mainly titanium, oxygen, and carbon.

The relevance of implant surface topography and how different levels of roughness, i.e., smooth (S_a < 0.5 μm), minimally rough (S_a = 0.5–1 μm), moderately rough (S_a > 1-2 μm), and rough (S_a > 2 μm), influence the bone response is heavily debated [28]. It is believed that moderately rough surfaces show a superior bone response to smoother or rougher surfaces [29]. According to a recent meta-analysis of studies using different types of clinically used implants, including 27 randomised controlled trials, smoother surfaces exhibited a higher tendency towards early failure compared

to rougher surfaces but also exhibited ~20% reduction in the risk of being affected by peri-implantitis, three years after loading [30]. The results of the present work are particularly noteworthy since relatively large differences in oxide thickness and surface roughness showed no differences in bone microarchitecture, ultrastructure, osteocyte morphology, and the molecular composition of the interfacial tissue after 12 weeks of healing. Furthermore, it appears likely that rendering a titanium surface mirror-like, by electropolishing, does not diminish the potential for titanium to support bone formation and/or bone remodelling, which is in contrast to the widely prevalent view that without appropriate surface modifications, titanium surfaces are "bioinert" and become encapsulated by fibrous tissue, in vivo [31, 32].

It is believed that nanostructuring enhances protein adsorption and guides cell-substrate interactions, in vitro [33, 34], thereby controlling not only cell adhesion but also differentiation, and may additionally confer antibacterial properties [35]. Although several recent experimental studies have demonstrated a thickened oxide layer to be advantageous for osseointegration of titanium implants [36, 37], the present work raises a fundamental question of whether or not there is a lower limit surface roughness at which titanium fails to osseointegrate. It may be speculated that the early bone response, that is, on the structural and molecular levels, may have been dissimilar for the two surfaces evaluated. However, any potential differences were lost following remodelling perhaps owing to the lack of a specific functional requirement. Due to technical limitations, ultrastructural evaluation using TEM could only be performed for the Ep surface. While it may be possible to obtain intact bone-implant specimens of the Ep+An surface for TEM using FIB-SEM, the technique permits analysis of relatively small regions of interest. Nevertheless, based on BSE-SEM, Raman spectroscopy, and resin cast etching, gross differences in the arrangement of structural components of the interfacial tissue (i.e., collagen fibrils and bone apatite) between Ep and Ep+An surfaces are not expected. The close proximity of osteocyte canaliculi to the smooth implant surface suggests the presence of a functioning mechanosensing apparatus irrespective of the oxide thickness and surface roughness at the nanometre level. Indeed, with S_a values $< 0.5\,\mu$m, both surfaces may be considered smooth. However, with the provision of primary stability, both surfaces supported bone formation and bone remodelling.

Finally, one distinct advantage of such smooth and relatively featureless implant surfaces is perceived to be the possibility of studying the physiological response to novel materials without the confounding effect of surface topography. Furthermore, in part due to the relative ease with which smooth implant surfaces may be separated from the tissue without disrupting the integrity of the tissue margin, such surfaces may lend themselves to the application of sample preparation techniques where a metal implant must be removed, for example, ultramicrotomed sections for transmission electron microscopy.

5. Conclusions

Despite the extremely smooth, mirror-like surface, electropolished titanium surfaces are able to support bone formation and remodelling, that is, osseointegration after 12 weeks in rabbit bone. The microstructure and composition of the interfacial tissue adjacent to thin surface oxide (4-5 nm) are similar to those adjacent to thicker surface oxide (180 nm). The close spatial relationship of osteocyte canaliculi and the implant surface suggests possible means of communication or mechanical load sensing irrespective of oxide thickness at the nanometre level.

Ethical Approval

The present animal experiments were performed according to the ethical standards set forth by the Animal Ethics Committee at the University of Gothenburg. These standards include rules to minimise stress and pain. The rules are implemented in the purchase, order, transport, handling, and maintenance of the animals prior to, during, and after any intervention. The experiments were under the surveillance of a qualified veterinarian.

Disclosure

The grant providers were not involved in the study design, data acquisition, interpretation, and writing and submission of the article.

Competing Interests

The authors confirm that there is no known conflict of interests associated with this publication and there has been no significant financial support for this work that could have influenced its outcome.

Acknowledgments

The authors wish to thank Lena Emanuelsson and Gunnel Bokhede for expert technical assistance. This study was supported by the BIOMATCELL VINN Excellence Center of Biomaterials and Cell Therapy, the Västra Götaland Region, the Swedish Research Council (Grant K2015-52X-09495-28-4), the ALF/LUA Research Grant "Optimization of Osseointegration for Treatment of Transfemoral Amputees" (ALFGBG-448851), the IngaBritt and Arne Lundberg Foundation, the Swedish National Association against Rheumatism, the King Gustaf V 80-Year Fund, the Dr. Felix Neubergh Foundation, the Promobilia Foundation, the Hjalmar Svensson Foundation, the Vilhelm and Martina Lundgren Vetenskapsfond, and the Materials Science Area of Advance at Chalmers and the Department of Biomaterials, University of Gothenburg.

References

[1] A. F. Mavrogenis, R. Dimitriou, J. Parvizi, and G. C. Babis, "Biology of implant osseointegration," *Journal of Musculoskeletal and Neuronal Interactions*, vol. 9, pp. 61–71, 2009.

[2] L. Le Guéhennec, A. Soueidan, P. Layrolle, and Y. Amouriq, "Surface treatments of titanium dental implants for rapid osseointegration," *Dental Materials*, vol. 23, no. 7, pp. 844–854, 2007.

[3] X. Liu, P. K. Chu, and C. Ding, "Surface modification of titanium, titanium alloys, and related materials for biomedical applications," *Materials Science and Engineering R: Reports*, vol. 47, no. 3-4, pp. 49–121, 2004.

[4] C. Larsson, P. Thomsen, J. Lausmaa, M. Rodahl, B. Kasemo, and L. E. Ericson, "Bone response to surface modified titanium implants: studies on electropolished implants with different oxide thicknesses and morphology," *Biomaterials*, vol. 15, no. 13, pp. 1062–1074, 1994.

[5] C. Larsson, P. Thomsen, B.-O. Aronsson et al., "Bone response to surface-modified titanium implants: studies on the early tissue response to machined and electropolished implants with different oxide thicknesses," *Biomaterials*, vol. 17, no. 6, pp. 605–616, 1996.

[6] P. Fratzl and R. Weinkamer, "Nature's hierarchical materials," *Progress in Materials Science*, vol. 52, no. 8, pp. 1263–1334, 2007.

[7] S. Weiner and H. D. Wagner, "THE MATERIAL BONE: structure-mechanical function relations," *Annual Review of Materials Science*, vol. 28, no. 1, pp. 271–298, 1998.

[8] R. Müller, "Hierarchical microimaging of bone structure and function," *Nature reviews. Rheumatology*, vol. 5, no. 7, pp. 373–381, 2009.

[9] P. Roschger, E. P. Paschalis, P. Fratzl, and K. Klaushofer, "Bone mineralization density distribution in health and disease," *Bone*, vol. 42, no. 3, pp. 456–466, 2008.

[10] J. Mahamid, B. Aichmayer, E. Shimoni et al., "Mapping amorphous calcium phosphate transformation into crystalline mineral from the cell to the bone in zebrafish fin rays," *Proceedings of the National Academy of Sciences of the United States of America*, vol. 107, no. 14, pp. 6316–6321, 2010.

[11] F. A. Shah, E. Zanghellini, A. Matic, P. Thomsen, and A. Palmquist, "The orientation of nanoscale apatite platelets in relation to osteoblastic–osteocyte lacunae on trabecular bone surface," *Calcified Tissue International*, vol. 98, no. 2, pp. 193–205, 2016.

[12] G. E. Fantner, H. Birkedal, J. H. Kindt et al., "Influence of the degradation of the organic matrix on the microscopic fracture behavior of trabecular bone," *Bone*, vol. 35, no. 5, pp. 1013–1022, 2004.

[13] D. B. Burr, "The contribution of the organic matrix to bone's material properties," *Bone*, vol. 31, no. 1, pp. 8–11, 2002.

[14] B. Depalle, Z. Qin, S. J. Shefelbine, and M. J. Buehler, "Large deformation mechanisms, plasticity, and failure of an individual collagen fibril with different mineral content," *Journal of Bone and Mineral Research*, vol. 31, no. 2, pp. 380–390, 2016.

[15] F. A. Shah, B. Nilson, R. Brånemark, P. Thomsen, and A. Palmquist, "The bone-implant interface—nanoscale analysis of clinically retrieved dental implants," *Nanomedicine: Nanotechnology, Biology, and Medicine*, vol. 10, no. 8, pp. 1729–1737, 2014.

[16] L. Sennerby, L. E. Ericson, P. Thomsen, U. Lekholm, and P. Astrand, "Structure of the bone-titanium interface in retrieved clinical oral implants," *Clinical Oral Implants Research*, vol. 2, no. 3, pp. 103–111, 1991.

[17] L. A. Giannuzzi and F. A. Stevie, "A review of focused ion beam milling techniques for TEM specimen preparation," *Micron*, vol. 30, no. 3, pp. 197–204, 1999.

[18] L. A. Giannuzzi, D. Phifer, N. J. Giannuzzi, and M. J. Capuano, "Two-dimensional and 3-dimensional analysis of bone/dental implant interfaces with the use of focused ion beam and electron microscopy," *Journal of Oral and Maxillofacial Surgery*, vol. 65, no. 4, pp. 737–747, 2007.

[19] K. Donath and G. Breuner, "A method for the study of undecalcified bones and teeth with attached soft tissues. The Säge-Schliff (sawing and grinding) technique," *Journal of Oral Pathology*, vol. 11, no. 4, pp. 318–326, 1982.

[20] F. A. Shah, X. Wang, P. Thomsen, K. Grandfield, and A. Palmquist, "High-resolution visualization of the osteocyte lacuno-canalicular network juxtaposed to the surface of nanotextured titanium implants in human," *ACS Biomaterials Science & Engineering*, vol. 1, no. 5, pp. 305–313, 2015.

[21] V. Mazet, C. Carteret, D. Brie, J. Idier, and B. Humbert, "Background removal from spectra by designing and minimising a non-quadratic cost function," *Chemometrics and Intelligent Laboratory Systems*, vol. 76, no. 2, pp. 121–133, 2005.

[22] T. Albrektsson, P.-I. Brånemark, H.-A. Hansson, and J. Lindström, "Osseointegrated titanium implants: requirements for ensuring a long-lasting, direct bone-to-implant anchorage in man," *Acta Orthopaedica Scandinavica*, vol. 52, no. 2, pp. 155–170, 1981.

[23] J. D. Currey, *Bones: Structure and Mechanics*, Princeton University Press, Princeton, NJ, USA, 2002.

[24] M. Haga, N. Fujii, K. Nozawa-Inoue et al., "Detailed process of bone remodeling after achievement of osseointegration in a rat implantation model," *Anatomical Record*, vol. 292, no. 1, pp. 38–47, 2009.

[25] R. M. Zebaze, A. Ghasem-Zadeh, A. Bohte et al., "Intracortical remodelling and porosity in the distal radius and post-mortem femurs of women: a cross-sectional study," *The Lancet*, vol. 375, no. 9727, pp. 1729–1736, 2010.

[26] P. Christen, K. Ito, R. Ellouz et al., "Bone remodelling in humans is load-driven but not lazy," *Nature Communications*, vol. 5, article 4855, 2014.

[27] F. A. Shah, M. L. Johansson, O. Omar et al., "Laser-modified surface enhances osseointegration and biomechanical anchorage of commercially pure titanium implants for bone-anchored hearing systems," *PLoS ONE*, vol. 11, no. 6, Article ID e0157504, 2016.

[28] A. Wennerberg and T. Albrektsson, "Effects of titanium surface topography on bone integration: a systematic review," *Clinical Oral Implants Research*, vol. 20, no. 4, pp. 172–184, 2009.

[29] T. Albrektsson and A. Wennerberg, "Oral implant surfaces: part 1-review focusing on topographic and chemical properties of different surfaces and in vivo responses to them," *International Journal of Prosthodontics*, vol. 17, no. 5, pp. 536–543, 2004.

[30] M. Esposito, Y. Ardebili, and H. V. Worthington, "Interventions for replacing missing teeth: different types of dental implants," *The Cochrane database of systematic reviews*, vol. 7, Article ID CD003815, 2014.

[31] J. B. Nebe, L. Müller, F. Lüthen et al., "Osteoblast response to biomimetically altered titanium surfaces," *Acta Biomaterialia*, vol. 4, no. 6, pp. 1985–1995, 2008.

[32] S. Nishiguchi, T. Nakamura, M. Kobayashi, H.-M. Kim, F. Miyaji, and T. Kokubo, "The effect of heat treatment on bone-bonding ability of alkali-treated titanium," *Biomaterials*, vol. 20, no. 5, pp. 491–500, 1999.

[33] S. Lavenus, J.-C. Ricquier, G. Louarn, and P. Layrolle, "Cell interaction with nanopatterned surface of implants," *Nanomedicine*, vol. 5, no. 6, pp. 937–947, 2010.

[34] E. Rieger, A. Dupret-Bories, L. Salou et al., "Controlled implant/soft tissue interaction by nanoscale surface modifications of 3D porous titanium implants," *Nanoscale*, vol. 7, no. 21, pp. 9908–9918, 2015.

[35] F. Varíola, F. Vetrone, L. Richert et al., "Improving biocompatibility of implantable metals by nanoscale modification of surfaces: an overview of strategies, fabrication methods, and challenges," *Small*, vol. 5, no. 9, pp. 996–1006, 2009.

[36] J. Yang, Y. Zhou, F. Wei, and Y. Xiao, "Blood clot formed on rough titanium surface induces early cell recruitment," *Clinical Oral Implants Research*, vol. 27, no. 8, pp. 1031–1038, 2016.

[37] M. Lennerås, A. Palmquist, B. Norlindh, L. Emanuelsson, P. Thomsen, and O. Omar, "Oxidized titanium implants enhance osseointegration via mechanisms involving RANK/RANKL/OPG regulation," *Clinical Implant Dentistry and Related Research*, vol. 17, supplement 2, pp. e486–e500, 2015.